Published in final edited form as:
J Biophotonics. 2014 August ; 7(8): 617–623. doi:10.1002/jbio.201300010.

M13 Virus based detection of Bacterial Infections in Living Hosts

Neelkanth M. Bardhan[1,2], **Debadyuti Ghosh**[1,2], and **Angela M. Belcher**[1,2,3,*]

[1] Department of Materials Science and Engineering, Massachusetts Institute of Technology, Cambridge, MA, USA

[2] The David H. Koch Institute for Integrative Cancer Research at the Massachusetts Institute of Technology, Cambridge, MA, USA

[3] Department of Biological Engineering, Massachusetts Institute of Technology, Cambridge, MA, USA

Abstract

We report a first method for using M13 bacteriophage as a multifunctional scaffold for optically imaging bacterial infections *in vivo*. We demonstrate that M13 virus conjugated with hundreds of dye molecules (M13-Dye) can target and distinguish pathogenic infections of *F*-pili expressing and *F*-negative strains of *E. coli*. Further, in order to tune this M13-Dye complex suitable for targeting other strains of bacteria, we have used a 1-step reaction for creating an anti-*bacterial antibody*-M13-Dye probe. As an example, we show anti-*S.aureus*-M13-Dye able to target and image infections of *S. aureus* in living hosts, with a 3.7x increase in fluorescence over background.

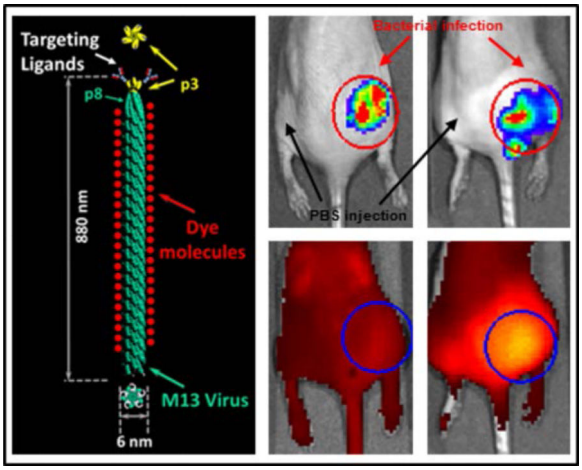

Keywords

M13 bacteriophage; optical imaging; fluorescent dye; bacterial infections

* Corresponding author: belcher@mit.edu, Phone: +1 (617) 324-2800, Fax: +1 (617) 258-6558.

Author biographies
Please see Supporting Information online.

1. Introduction

The ability to image and noninvasively monitor bacterial infections in tissue has been a challenging area in the field of pathology. The increasing development of bacterial resistance to antibiotics has reached high proportions, and thus there is a need for imaging tools to facilitate early detection and treatment of bacterial infections. In the US alone, the economic impact of antibiotic-resistant bacterial infections is estimated ~$5-$24 billion per year [1].

Optical imaging of bacteria *in vivo* is much less developed than other methods such as radioimaging [2], [3]; due to lack of availability of target-specific molecular probes. One early approach was using genetic reporter systems such as light-emitting luciferase enzymes [4], or green fluorescent protein (GFP). Although this has proved to be an important tool for visualizing bacteria, these reporters are not endogenously expressed in most pathogens. Therefore, there is a need for developing bacterial targeting probes with exogenous contrast agents for optical imaging.

Several studies have employed antibodies, lectins, sugars, antibiotic drugs, enzyme substrates and antimicrobial peptides [5],[6], cell-wall penetrating cationic peptides [7],[8] and specifically constructed compounds [9],[10],[11] as affinity ligands for targeting bacteria. While these are promising candidates for imaging bacterial infections, there are still doubts concerning the specificity of some of these probes, due to the possibility of the ligand targeting the adjacent necrotic tissue produced by the infection [9]. In contrast, probes based on antibody-mediated targeting are a popular choice because they can bind tightly to specific molecular targets on the surfaces of both Gram-positive and Gram-negative bacteria.

M13 bacteriophage is an attractive candidate for targeting bacterial infections, because of its natural binding affinity to bacteria which express *F*-pili, and its five capsid proteins which can be genetically engineered to display targeting motifs against tumor cells [12],[13], drug molecules or fluorescent dyes [14] for strain-specific detection and imaging of bacteria. Although M13 has been used for detection of tumors [13],[15], gene delivery methods for phage therapy [16],[17],[18] and in antibiotic therapy [19] for treating bacterial infections in survival studies, there has been no reported application of M13 used as a targeted *in vivo* imaging probe for infectious diseases, to the best of our knowledge. In this work, we describe a first approach to using M13 as a multifunctional scaffold, fluorescently labeled with dye molecules, for targeting and imaging bacterial infections.

2. Experimental

2.1 Labeling of Fluorescent Dye on M13 phage

M13 virus was suspended at a concentration of 3×10^{13} pfu/mL (plaque forming units per mL) in 1x phosphate buffered saline (PBS). Alexa Fluor 750 dye was used (Life Technologies, NY, USA), with an absorbance maximum at 749nm, and emission maximum at 775nm. After reacting the dye with M13 for 2hr in dark, the solution was dialyzed extensively against 1x PBS for 48hr, to remove unreacted dye molecules. After dialysis, the

M13-Dye complex was precipitated by adding high ionic strength salt solution of PEG-NaCl (2M) at 4°C, and centrifuged at 15,000rpm for 10min. The supernatant was discarded to get rid of unreacted dye molecules, and the M13-dye pellet was resuspended in 1x PBS. After 3 such steps, absorption spectra were taken with a DU-800 Spectrophotometer (Beckman Coulter, CA, USA).

2.2 Cell Lines and Culture

E. coli of two strains, DH5-α (New England Biolabs, MA, USA) and JM109 (Promega, WI, USA) were used, of which the former lacks *F*-pili, the latter is *F*-pilus positive. We used Xen-29 strain of *Staphylococcus aureus*, and Xen-05 strain of *Pseudomonas aeruginosa* (Caliper Life Sciences, MA, USA). All bacteria were grown in LB broth, with 50 μg/mL tetracycline for the *E. coli* and *P. aeruginosa* strains, and 50 μg/mL kanamycin for *S. aureus*. The bacteria were grown in an incubator at 37°C under vigorous shaking at 250rpm, till O.D.600 absorbance attained a value of 0.5.

2.3 In vitro Binding Assay

Bacterial strains were grown to a density of 10^8 cfu/mL (colony forming units per mL) in LB media. 100μL of this culture was added per well, of a 96-well plate. Depending on the strain of bacteria, we added our probe (M13-Dye for the *E. coli* strains JM109 or DH5-α, and anti-*S.aureus*-M13-Dye for the *S. aureus* strain Xen-29). As negative controls, we used free dye in PBS. The probe was incubated with the bacteria for 1hr. in the culture medium. After 1hr., we centrifuged the plate to sediment the bacteria. The unbound bacteria and unattached probe were removed by 3 PBS wash steps. Finally the cells were resuspended in 100μL PBS. Fluorescence images were taken on a Xenogen IVIS imaging instrument (Caliper Life Sciences, MA, USA).

2.4 1-step Tunability of M13 Phage

In order to enable the M13 phage to selectively conjugate to other strains of bacteria which do not natively have *F*-pili, we used a 1-step tuning process. Previously [15], a method has been reported to express biotin acceptor peptide (BAP), GLNDIFEAQKIEWHE [20], on the p3 coat protein of the M13 bacteriophage. M13 viruses expressing BAP (BAP-M13) were then enzymatically biotinylated at the lysine residue (Lys10) using a biotin-protein ligase (Avidity, CO, USA). Antibodies against bacteria were complexed to streptavidin using a commercially available kit (EasyLink Streptavidin kit, abcam, Cambridge, MA). This complex was then reacted with biotinylated BAP-M13 to develop probes (*antibacterial antibody*-M13-Dye) for targeting against specific bacterial infections.

2.5 Mouse Handling and Fluorescence Whole-Animal Imaging

All animal handling procedures were done in accordance with Institutional Animal Care and Use Committee protocols. Animal procedures were pre-approved by the Massachusetts Institute of Technology's Committee on Animal Care.

For infection studies, 43-56 days old female nude nu/nu mice were used (strain 088, Charles River Laboratories, MA, USA). Two sets of experiments were performed, involving *E. coli* and *S. aureus* strains. For each strain, two groups of N=5 mice were studied. In the first set,

one group received the DH5-α strain, and the second group received JM109. In the second set, all mice received the Xen-29 strain. 10^8 cells of bacteria in 50μL LB media were injected in the right caudal thigh muscle using a 25 gauge needle. As a control, 50μL of 1x PBS was also injected in the left thigh. As a second negative control test for our probe specificity, 5×10^7 cells of *P. aeruginosa* were injected in *N*=5 mice. For the mice injected with *S. aureus* or *P. aeruginosa*, the bacterial infection was visualized by bioluminescence imaging (IVIS Spectrum, Caliper Life Sciences, MA, USA). After incubating the bacteria in the living host for 1hr., 200μL of the M13-Dye probe (or anti-*S.aureus*-M13-Dye for the positive control group of the *S. aureus* set and the negative control *P. aeruginosa* set) was injected into the circulation through a retro-orbital injection. The time of injection of the M13-Dye probe was taken as $t = 0$. Post injection, mice were imaged at t = 1hr, 2, 4, 8, 12 and 24hr. on the IVIS instrument, using a 745nm excitation and an 800nm fluorescence emission filter.

Post this imaging sequence, mice were euthanized by CO_2 inhalation. We collected muscle tissue from the right flank (site of bacterial infection) and left flank (negative control PBS injection). Fluorescence images of as-excised tissues were taken on the IVIS instrument. After imaging, the excised tissues were fixed in 10% formalin and mounted in paraffin wax.

2.6 Microscopy Analysis

5μm tissue sections were mounted on glass slides and stained with Gram staining kit (Sigma-Aldrich, St. Louis, MO). They were imaged with a Zeiss Axioplan II upright microscope with objective lenses of 25x and 100x magnification, under oil-immersion.

3. Results and discussion

M13 is a long, cylindrical filamentous non-lytic bacteriophage. Figure 1a shows the typical structure of M13 loaded with near-infrared dye molecules attached to the p8 coat protein (M13-Dye). Figure 1b shows absorbance spectrum measured to quantify the labeling of dye molecules on the M13 phage. From the absorption value at λ = 269nm, compared to a 320nm reference [21], the phage concentration was determined to be 3×10^{13} pfu/mL. The Alexa Fluor 750 dye has an absorption maximum at λ_{max} = 749nm, with an extinction coefficient ε = 240,000 $cm^{-1}M^{-1}$. We measure an absorbance value A = 1.76, for a path length l = 1cm. Using the Beer-Lambert law $A = \varepsilon lc$, we calculate the concentration of the dye to be c = 7.33μM, or equivalently, 4.42×10^{15} dye molecules per mL. Therefore, the average number of dye molecules per phage works out to be ~150. This ability to conjugate hundreds of dye molecules through high avidity binding on a single carrier vector (M13) for targeting and signal amplification at the site of bacterial infection is one of the key advantages of our M13-Dye system, similar to effects observed when using M13 for delivering magnetic nanoparticles for imaging [22]. Following the M13-Dye conjugation reaction, the product was dialyzed extensively and followed with several rounds of precipitation to remove excess, unreacted dye molecules. Inset to Figure 1b shows the clear supernatant after precipitating the blue pellet of M13-Dye, indicated by the yellow arrow. There is very little residual absorption measured in the supernatant, indicating that there is no unbound dye detectable. Figure 2 shows the results of our plate assay to determine the binding affinity of our M13-Dye complex to different strains of bacteria. For the *E. coli*

strains, from Figure 2a it is observed that M13-Dye binds specifically to the *F*-positive JM109, with a 2.3x increase in fluorescence intensity over the *F*-negative DH5-α strain. There is slight nonspecific binding in the latter, which has a higher fluorescence intensity compared to the background intensity of free dye in PBS (control).

Further, we have conjugated an antibody against *S. aureus* on the M13-Dye probe (anti-*S.aureus*-M13-Dye). Figure 2b shows the results of our *in vitro* binding assay. We observe a 3.3x increase in binding to *S. aureus* by the antibody-conjugated anti-*S.aureus*-M13-Dye complex, over the M13-Dye alone. The latter has a slight non-specific binding to *S. aureus*, ~1.5x compared to free dye in PBS (control).

This ability to modulate the binding affinity of our M13-Dye complex simply by adding a suitable antibody on the p3 is another key advantage, which makes our probe versatile for detecting a wide range of infectious pathogens.

Based on the outcome of our *in vitro* plate assay, we tested the ability of our M13-Dye conjugate to target and locate the site of bacterial infection in living hosts. In order to determine the optimum time for fluorescence intensity comparison, we first performed a study of the time-course of circulation and uptake of our M13-Dye probe. Figure 3 shows a subset of the results of our time-course imaging. At $t = 0$ post injection (p.i.), we observe diffuse fluorescence throughout the whole body, as the probe is under circulation. Specific organs such as the liver and spleen are also visible in some cases. With time, the probe starts clearing from circulation, and accumulation is observed at the site of infection. The peak accumulation is observed to occur around $t = 8$hr. for the *S. aureus* infections, and $t = 24$hr. for the *E. coli* infections, shown in Figure 3. Beyond this peak signal, the fluorescence intensity starts decreasing, although the infection site is still distinguishable at later times. We propose that the optimal wait times for targeted imaging are 24hr. and 8hr., for the *E. coli* infections and *S. aureus* infections respectively.

We compared the fluorescence signal intensity of our M13-Dye probe, for targeted and non-targeted cases, and measured the increase in fluorescence compared to PBS injections in the left flank (control). These measurements were performed at the time of peak intensity, i.e. at $t = 8$hr. for the *S. aureus* injections, and $t = 24$hr. for the *E. coli* injections and the negative control *P. aeruginosa* injections. Region of interest (ROI) analysis was performed on these groups, to determine the Target/PBS and Non-Target/PBS fluorescence ratios, as shown in Figure 4a. Also shown are the bioluminescence images of the Xen-29 bacteria, showing colocalization of the probe accumulation at the site of bacterial infection.

Figure 4b shows the results of our ROI analyses. We discuss the positive controls first (JM109 v. M13-Dye and Xen-29 v. anti-*S.aureus*-M13-Dye). For the *E. coli* strain JM109, which is *F*-positive, we observe a 2.7x increase in intensity compared to control PBS. For the *S. aureus* strain Xen-29, targeted using an anti-*S.aureus* antibody conjugated to the M13-Dye, we observe a stronger enhancement ~3.7x compared to PBS control. Both the non-targeted negative controls (DH5-α v. M13-Dye and Xen-29 v. M13-Dye) show a 1.3-1.5x increase in intensity over PBS control, which suggests minor non-specific binding of our probe. These results compare to similar ratios of targeting observed in our *in vitro* assays,

shown in Figure 2. To assess the specificity of our anti-*S.aureus*-M13-Dye probe, we injected it into mice infected with *P. aeruginosa.* We observe a fluorescence enhancement of ~1.2x over PBS control, which is comparable to the other negative control cases discussed above. It may be observed that the increases in fluorescence intensity for the targeted cases are slightly lower for whole-animal imaging compared to plate assays. This may be attributed to the slower rate of targeting through circulation. We observe an enhancement factor closer to the *in vitro* results upon excising the tissue, as shown in Figure 5.

In order to further verify the uptake of our M13-Dye probe and eliminate false positives, we sacrificed the animals after t = 24hr. Tissue samples from both the right flank (site of infection) and the left flank (PBS control) were excised and fluorescence images were taken. Figure 5a shows the ROI analysis performed (blue outlines). Columns 1 and 3 of the plate correspond to PBS-injected tissues, while 2 and 4 are the targeted infection samples. We observe a 4.1x increase in fluorescence intensity in the targeted tissues, compared to tissues receiving control PBS injections. This compares favorably with our ROI analysis of whole-animal images in Figure 4b, which yielded a 3.7x increase. This enhancement factor is closer to the 4.9x increase observed for anti-*S.aureus*-M13-Dye in the plate assay results of Figure 2b.

Further, these tissue samples were sectioned and stained for Gram-positive bacteria, shown in Figure 5b. For the left muscle, we observe no evidence of staining. For the right flank muscle tissues, we see presence of clusters of spherical cocci of *S. aureus* stained dark violet, interspersed throughout the muscle tissue fibers. At 100x magnification, individual cells of *S. aureus* are resolved, with sizes ranging from 0.5-0.8μm, similar to images reported in literature [23]. The two observations of Figure 5a and 5b, combined together with the whole-animal images of Figure 4, help us validate the targeting capability of our anti-*S.aureus*-M13-Dye probe towards *in vivo* infections of *S. aureus.*

4. Conclusion

In this study, we have demonstrated a multifunctional, targeted, highly tunable composite material, using M13 bacteriophage as a carrier vector, labeled with fluorescent dye molecules (M13-Dye), for detecting and imaging pathogenic infections in living hosts. The ability to attach hundreds of dye molecules onto a single carrier vector is one of the key advantages of our system. We have shown the ability to distinguish infections *in vivo*, between strains of *E. coli* which express *F*-pili appendages (such as JM109), from *F*-negative ones (like DH5-α), with a 2.7x increase in fluorescence intensity over negative control PBS injections.

Further, we have developed a 1-step process to enable the M13 virus to selectively attach to strains of bacteria which do not express *F*-pili. Using an anti-*S.aureus*-M13-Dye probe, we have shown the ability to selectively localize and target infections of *S. aureus in vivo*, with a fluorescence signal ~3.7x higher than that of control PBS injections, and a 2.5x increase over non-targeted M13-Dye. These results are corroborated through the analyses of integrated fluorescence intensity observed in the excised tissue. This ability to tune the

targeting motif of the M13 carrier through a simple 1-step antibody modification is one of the key advantages of our M13-Dye probe system.

This work may potentially be extended in the future by engineering the M13 virus to attach single-wall carbon nanotubes as an imaging probe for second-window near-infrared imaging [15] for visualization of deeper infections in tissue, include delivery of antibiotics, gene delivery, or phage therapy, for a complete diagnostics and therapy package solution.

Supplementary Material

Refer to Web version on PubMed Central for supplementary material.

Acknowledgments

This work was supported by funding from the National Cancer Institute Center for Cancer Nanotechnology Excellence (grant 5-U54-CA151884-03). N.M.B. would like to acknowledge Kris Hewes, Cassandra Miller and Sarah Ambrose of MIT's Department of Comparative Medicine for assistance with injections and tissue harvesting. We thank Scott Malstrom from the Applied Therapeutics and Whole Animal Imaging Core of the Koch Institute's (KI) Swanson Biotechnology Center, for help with the IVIS imaging system. We also acknowledge Kathy Cormier from the Histology Core of the KI Swanson Biotech Center for assistance with staining, and Eliza Vasile of the KI Microscopy facility.

References

1. Hall BG. Nat Rev Micro. 2004; 2(5):430–435.
2. Rennen HJ, Boerman OC, Oyen WJ, Corstens FH. Eur J Nucl Med. 2001; 28(2):241–252. [PubMed: 11303896]
3. Bettegowda C, Foss CA, Cheong I, Wang Y, Diaz L, Agrawal N, Fox J, Dick J, Dang LH, Zhou S, Kinzler KW, Vogelstein B, Pomper MG. Proceedings of the National Academy of Sciences of the United States of America. 2005; 102(4):1145–1150. [PubMed: 15653773]
4. Contag CH, Contag PR, Mullins JI, Spilman SD, Stevenson DK, Benaron DA. Molecular Microbiology. 1995; 18(4):593–603. [PubMed: 8817482]
5. Lupetti A, Mick M, Welling, Ulderico. European Journal of Nuclear Medicine and Molecular Imaging. 2002; 29(5):674–679. [PubMed: 11976807]
6. Welling MM, Paulusma-Annema A, Balter HS, Pauwels EK, Nibbering PH. Eur J Nucl Med. 2000; 27(3):292–301. [PubMed: 10774881]
7. Nekhotiaeva N, Elmquist A, Rajarao GK, Hällbrink M, Langel Ü, Good L. The FASEB Journal. 2004; 18(2):394–396.
8. Bullok KE, Gammon ST, Violini S, Prantner AM, Villalobos VM, Sharma V, Piwnica-Worms D. Mol Imaging. 2006; 5(1):1–15. [PubMed: 16779965]
9. Leevy WM, Gammon ST, Jiang H, Johnson JR, Maxwell DJ, Jackson EN, Marquez M, Piwnica-Worms D, Smith BD. J. Am. Chem. Soc. 2006; 128(51):16476–16477. [PubMed: 17177377]
10. Leevy WM, Gammon ST, Johnson JR, Lampkins AJ, Jiang H, Marquez M, Piwnica-Worms D, Suckow MA, Smith BD. Bioconjugate Chem. 2008; 19(3):686–692.
11. Ning X, Lee S, Wang Z, Kim D, Stubblefield B, Gilbert E, Murthy N. Nat Mater. 2011; 10(8):602–607. [PubMed: 21765397]
12. Krag DN, Shukla GS, Shen G-P, Pero S, Ashikaga T, Fuller S, Weaver DL, Burdette-Radoux S, Thomas C. Cancer Research. 2006; 66(15):7724–7733. [PubMed: 16885375]
13. Kelly, KA.; Waterman, P.; Weissleder, R. Neoplasia. Vol. 8. New York, NY: 2006. p. 1011-1018.
14. Ghosh D, Kohli AG, Moser F, Endy D, Belcher AM. ACS Synth. Biol. 2012; 1(12):576–582. [PubMed: 23656279]
15. Yi H, Ghosh D, Ham M-H, Qi J, Barone PW, Strano MS, Belcher AM. Nano Lett. 2012; 12(3): 1176–1183. [PubMed: 22268625]

16. Barry MA, Dower WJ, Johnston SA. Nature Medicine. 1996; 2(3):299–305.
17. Lu TK, Collins JJ. Proceedings of the National Academy of Sciences. 2009 doi: 10.1073/pnas.0800442106.
18. Capparelli R, Parlato M, Borriello G, Salvatore P, Iannelli D. Antimicrobial Agents and Chemotherapy. 2007; 51(8):2765–2773. [PubMed: 17517843]
19. Yacoby I, Shamis M, Bar H, Shabat D, Benhar I. Antimicrobial Agents and Chemotherapy. 2006; 50(6):2087–2097. [PubMed: 16723570]
20. Beckett D, Kovaleva E, Schatz PJ. Protein Sci. 1999; 8(4):921–929. [PubMed: 10211839]
21. Day LA. Journal of Molecular Biology. 1969; 39(2):265–277. [PubMed: 5362671]
22. Ghosh D, Lee Y, Thomas S, Kohli AG, Yun DS, Belcher AM, Kelly KA. Nature Nanotechnology. 2012; 7(10):677–682.
23. Lowy FD. New England Journal of Medicine. 1998; 339(8):520–532. [PubMed: 9709046]

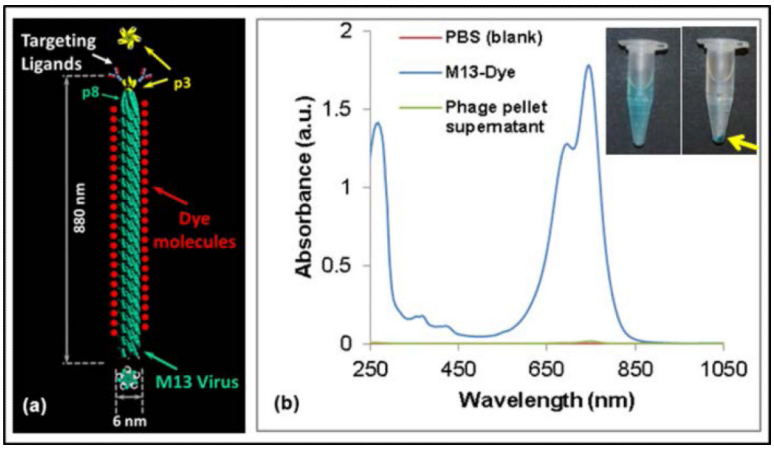

Figure 1.

(a) Schematic structure of the M13 bacteriophage, rendered in green. Typical dimensions are ~880 nm in length and ~6 nm in diameter. The major coat protein p8 binds to several hundred dye molecules, shown in red. At one end is the minor coat protein, p3, which can be used to conjugate targeting ligands such as antibodies. (b) Absorbance spectra of M13-Dye (blue curve). Inset shows the M13-Dye solution (*left*, blue liquid), and the clear supernatant after precipitation thrice with PEG-NaCl (*right*, yellow arrow indicates phage pellet). There is negligible residual absorption from the supernatant (green curve), indicating no unbound free dye detected.

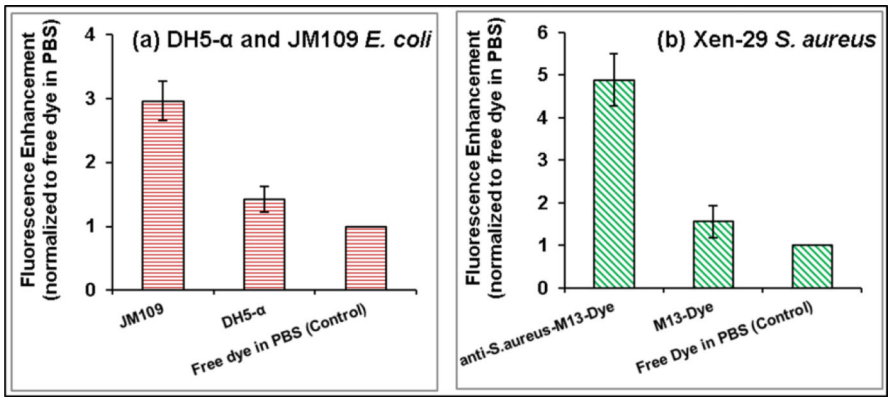

Figure 2.

Plate assay quantifying the binding affinity of M13-Dye probe to different strains of bacteria. Each data point is the mean ±s.d. for *n*=6 wells. (a) M13-Dye binds to *E. coli* strain JM109, which is *F*-positive, with a 2.3x increase in fluorescence intensity over *F*-negative DH5-α. (b) anti-*S.aureus*-M13-Dye binds strongly to *S. aureus* strain Xen-29, with a 3.3x increase compared to the non-targeted M13-Dye.

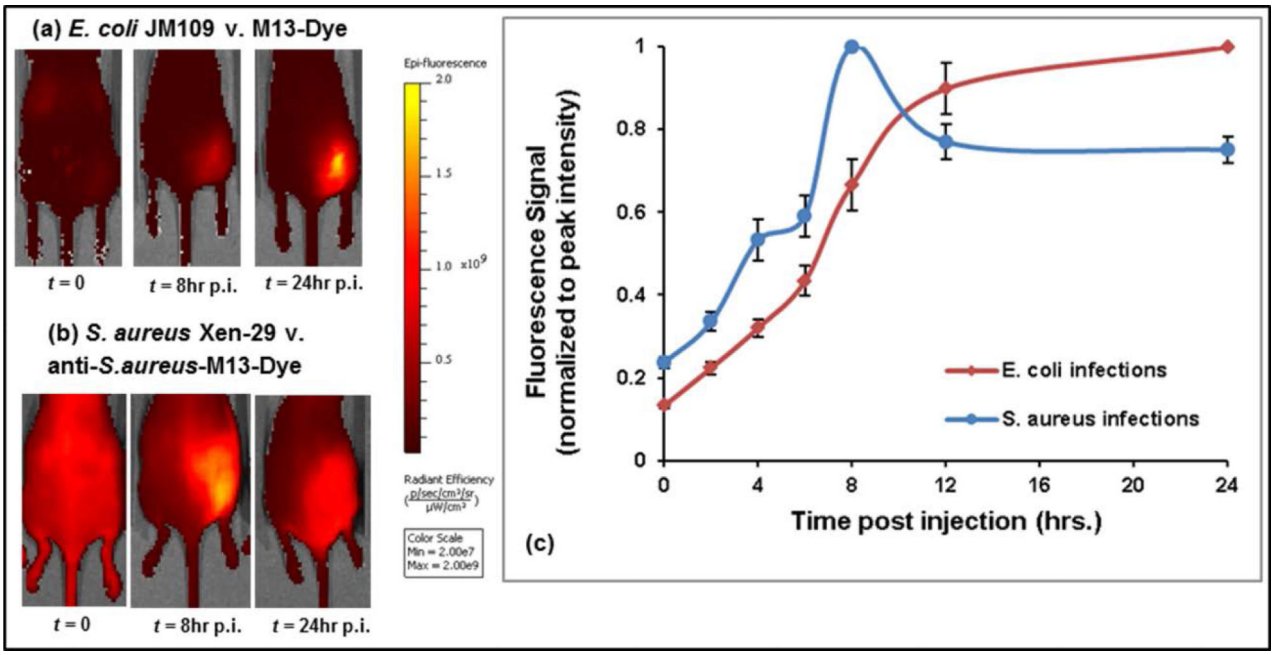

Figure 3.

Optical clearance profile of circulation and uptake of the M13-Dye probe, for the positive control samples. One representative mouse is shown out of a cohort of *N*=5 samples for each set. (a) For the *E. coli* strains, maximum uptake at the site of infection is observed at *t* = 24hr. post injection (p.i.). (b) For the *S. aureus* strain, maximum uptake is at *t* = 8hr. p.i. All samples are normalized to the same range. The radiant efficiency scale reads 2E7-2E9 (photons/sec/cm^2/sr)/(μW/cm^2). (c) Fluorescence intensity at site of infection, normalized to peak uptake, with time p.i.

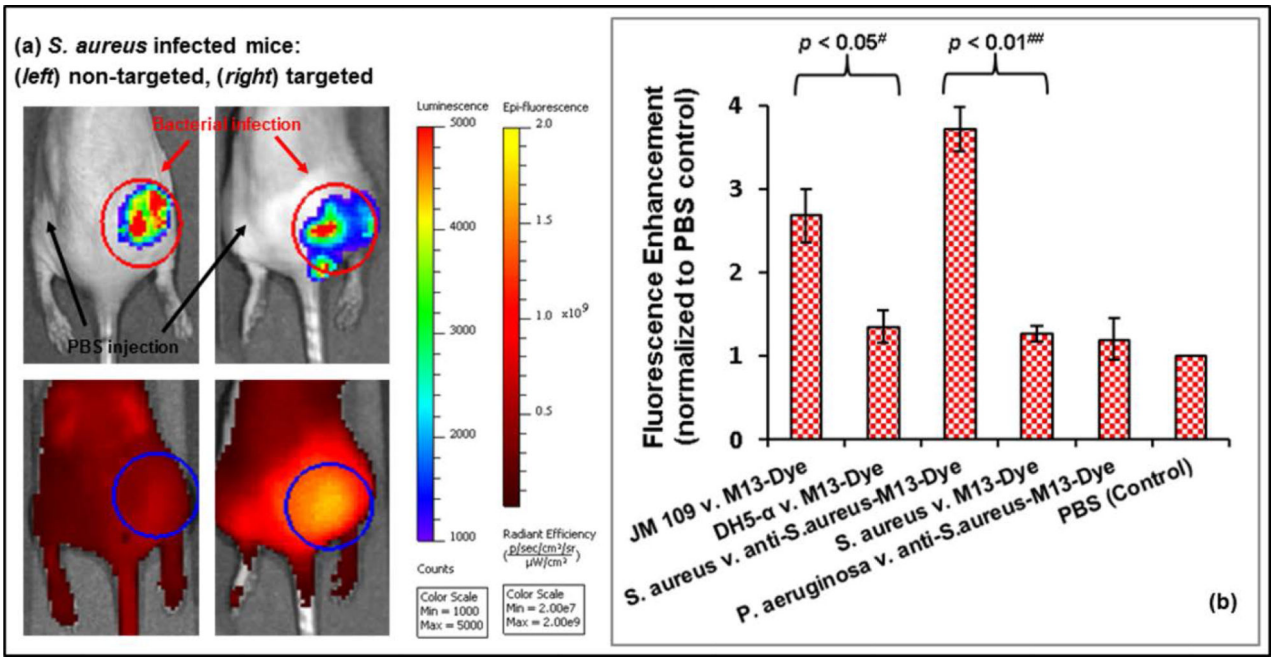

Figure 4.

Specificity of uptake of the M13-Dye probe. (a) One representative mouse from each group of *N*=5 mice injected with *S. aureus* is shown here. (*top*) Bioluminescent image from Xen-29 bacteria. (*bottom*) Fluorescence of the M13-Dye based probe. The left panel mouse is a non-targeted case (M13-Dye injection), while on the right is a targeted case (anti-*S.aureus*-M13-Dye). The bioluminescence scale reads from 1000-5000 (Counts). The fluorescence scale is 2E7-2E9 (photons/sec/cm^2/sr)/(μW/cm^2). ROI analysis was performed, indicated by the blue circles, with a threshold set at 25% of maximum intensity. For comparison, ROIs were taken to be of equal area, between target and non-target groups. Similar analysis was performed with the mice injected with strains of *E. coli* (not shown here). (b) Fluorescence signal (right flank) intensity enhancement, normalized to baseline intensity (control PBS injections in left flank) plotted as mean ±s.d. of *N*=5 measurements. #, ##: Student's *t*-test for paired data with one-tailed distribution.

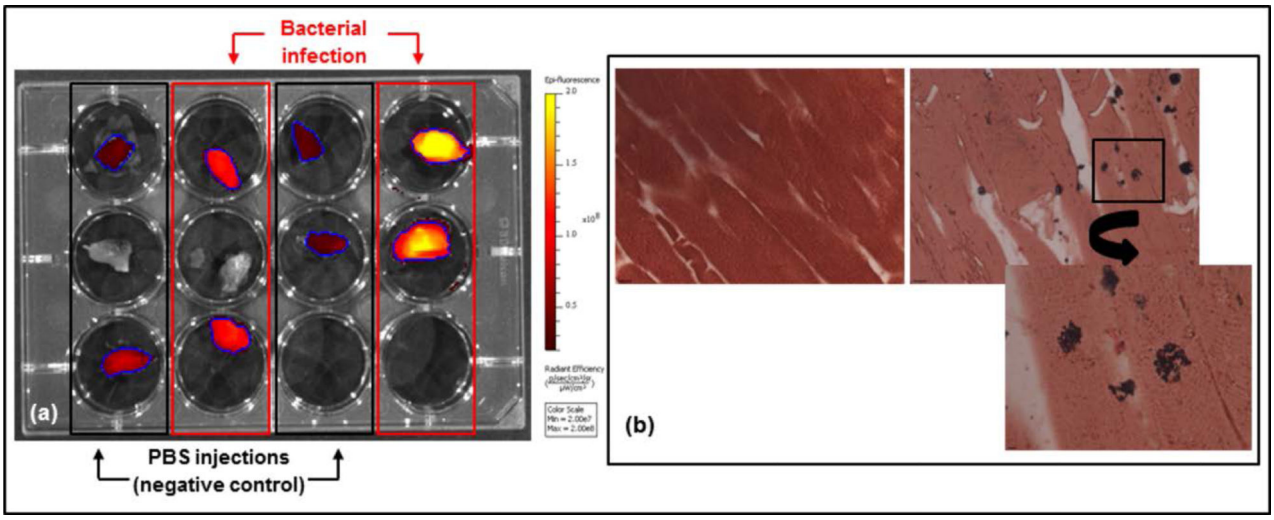

Figure 5.

(a) Representative ROI analysis of excised muscle tissue for the positive control group (anti-*S.aureus*-M13-Dye). One mouse was not injected with the probe. Because of the uneven sizes of the excised tissue, an auto contour mapping function was used to determine the ROIs (blue outlines). (b) Tissue sections with Gram staining, 25x objective, oil-immersion lens. The scale bar is 15μm. (*left*) Muscle tissue taken from left flank (PBS control), (*right*) muscle tissue from the right flank (bacterial injection). Inset shows part of the same sample at 100x objective (scale bar is 3μm).